AUTOPARAMETRIC RESONANCE IN A PIEZOELECTRIC MEMS VIBRATION ENERGY HARVESTER

Yu Jia[1,2], Sijun Du[1], Emmanuelle Arroyo[1] and Ashwin A. Seshia[1]
[1]Nanoscience Centre, University of Cambridge, Cambridge, UK
[2]Department of Mechanical Engineering, University of Chester, Chester, UK

ABSTRACT

This paper reports for the first time the achievement of autoparametric resonance in a piezoelectric MEMS energy harvester without compromising transducer strain energy optimisation, in order to enhance the efficiency of vibration energy harvesting. The autoparametrically driven energy harvester in excess of a two-fold increase in power output than the same device driven into direct resonance at the same acceleration level, and about an order of magnitude higher in power density normalised to acceleration squared relative to the state-of-the-art.

INTRODUCTION

Vibration energy harvesting (VEH) aims to harness ambient kinetic energy and output useful electrical energy via a suitable transducer such as one based on piezoelectricity. MEMS VEH offers the potential promise of providing a fully integrated and self-sustaining power source for embedded microsystems. Generally, direct resonance has been employed as the default method of resonant amplification to harvest external excitations.

Previously [1, 2], parametrically excited electrostatic MEMS VEH devices have demonstrated over an order of magnitude higher in both power output and frequency bandwidth over direct resonance. By employing an instability phenomenon, parametric resonance has a fundamental theoretical advantage over direct resonance as a means of accumulating mechanical energy.

However, a non-trivial damping-dependent initiation threshold needs to be first attained. While this technical limitation has since been successfully overcome with the inclusion of a passive initial spring design for electromagnetic and electrostatic transducers [3], further operational challenges still remain for piezoelectric implementations [3, 4]. Despite the successful activation of parametric resonance for piezoelectric oscillators [3, 4], the additional initial spring feature adversely concentrates the resultant strain energy over a small localised area and thus compromises the piezoelectric transducer output.

This paper presents for the first time, a topology to achieve parametric resonance for piezoelectric MEMS VEH without sacrificing strain distribution for a given transducer area. Therefore, this design enables the practical implementation of a more efficient resonant mechanical amplifier for piezoelectric MEMS VEH.

DESIGN AND SIMULATION

An auto-parametric oscillator, such as [4], contains a directly excited oscillator sub-system that is internally coupled to a parametric oscillator sub-system with a 2:1 frequency ratio. The dynamics of these devices can be modelled by nonlinear coupling [5] between the two modes. The secondary mode is autoparametrically excited via nonlinear coupling to a directly driven primary mode.

Figures 1 and 2 illustrate the design and simulated modal response of the proposed coupled oscillator topology to achieve autoparametric resonance.
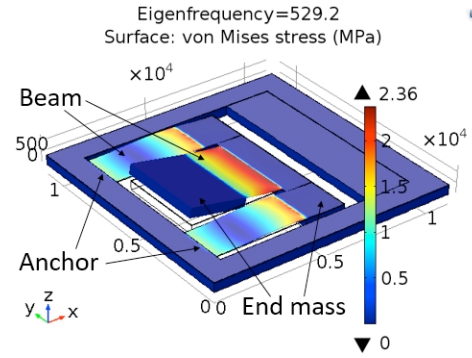

Figure 1: Simulation of the transverse mode (f_1) of the coupled direct cantilever within the MEMS autoparametric oscillator topology.
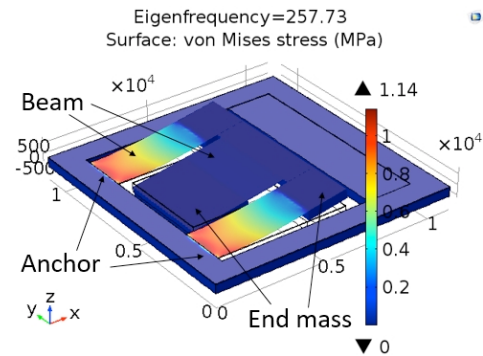

Figure 2: Simulation of the transverse mode (f_2) of the first parametric cantilever within the MEMS autoparametric coupled oscillator topology.

The device consists of a dual-arm primary cantilever, an end mass that strongly couples the two arms, and a subsidiary secondary cantilever with its own end mass extending from the first end mass. Therefore, the oscillations of the two cantilevers are mutually coupled. When the resonant frequencies f_1 and f_2 are matched to a precise ratio of 2:1, autoparametric oscillation can onset as the oscillation of secondary cantilever acts as an internal periodic parameter modulation ($f_1 = 2f_2$) for the primary cantilever.

As the secondary cantilever is driven into direct resonance by external excitation, its oscillation then parametrically drives the primary cantilever into autoparametric resonance. Following this, the resonant amplitude growth of the directly excited secondary cantilever is clamped and energy is pumped into the primary cantilever irrespective of linear damping.

METHOD

The piezoelectric MEMS devices were fabricated using a 3 μm AlN on 25 μm SOI process summarised in Figure 3. The top electrode is an Al layer. A doped Si device layer acts as both the mechanical device layer as well as the bottom electrode layer. End masses were formed from un-etched regions of the silicon wafer.
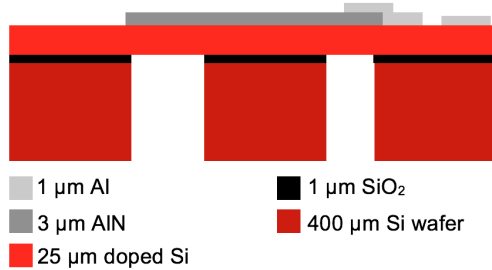

▨ 1 μm Al		▬ 1 μm SiO₂	
▨ 3 μm AlN		▬ 400 μm Si wafer	
▬ 25 μm doped Si			

Figure 3: Stack of material used in the piezoelectric MEMS fabrication process.

Figure 4 presents the fabricated MEMS device fixed within a leadless chip carrier using epoxy adhesive. A spacer of 1 mm thickness, around the boundary of the die, was placed beneath the die in order to allow shuttle travel. Al wire bonds were used to route out the transducer output from the Al bond pads.
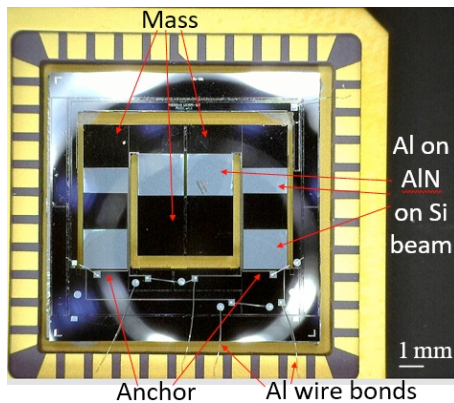

Figure 4: View of fabricated piezoelectric (AlN-on-Si) MEMS device, fixed within a chip carrier.

As shown in Figure 5, the electrical connections result in three distinct piezoelectric regions: (i) beam bending of the first cantilever, (ii) end mass induced anchor strain on the first cantilever when the second cantilever is driven into resonance, and (iii) beam bending of the second cantilever. Electrical interconnects to the three electrode regions were separated in order to prevent strain charge cancellation. However, the first two regions are from the same cantilever beam and does not have a phase delay. Therefore, the two regions can be connected in series when the secondary cantilever is oscillating.
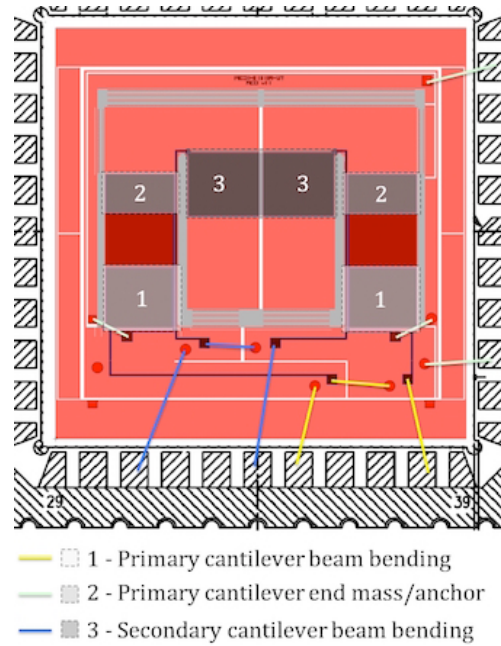

— ▨ 1 - Primary cantilever beam bending
— ▨ 2 - Primary cantilever end mass/anchor
— ▨ 3 - Secondary cantilever beam bending

Figure 5: Wire bonding diagram to electrically route the various piezoelectric strain regions from the autoparametric MEMS device.

The electrode layer only covers the areas of high induced strain (60% of from the peak) based on a previous optimisation study [6]. Figure 6 shows the simulated strain areas that advised on the design of the electrode area size. This topology thus allows for the distribution of induced strain energy across a substantial transducer area.
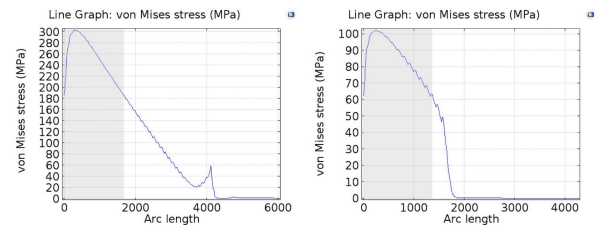

Figure 6: Simulation of the strain response of the primary cantilever (left) and secondary cantilever (right) when they are individually in resonance. Grey region shows the effective transducer areas that are profitable to harvest.

The experimental setup is shown in figure 7. The chip carrier sits within a socket, which is fixed onto a mechanical shaker. The device is driven in air using by the shaker, which is controlled by a function generator. The input base vibration level is measured by a 3-axis MEMS accelerometer. The output of the MEMS device and the accelerometer are simultaneously logged on a digital oscilloscope.
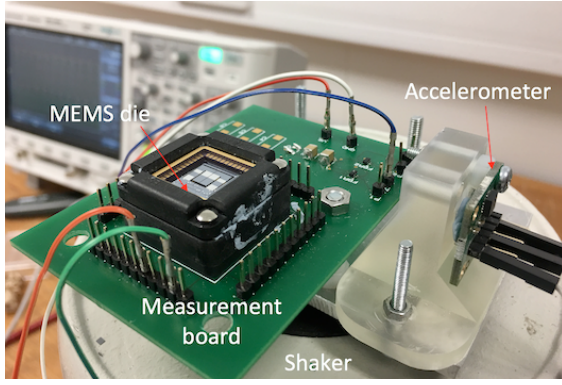
Figure 7: View of the experimental vibration setup used to characterise the MEMS VEH devices.

EXPERIMENTAL RESULTS

While f_1 and f_2 were designed to match the autoparametric ratio, fabrication tolerances in the processing resulted in device variations across different regions on the wafer. The experimental characterisation revealed varying degrees of detuning. Two of the MEMS devices are reported here and their frequency values summarised in Table 1.

Table 1. Resonant frequencies of MEMS devices.

MEMS VEH devices	f_1 (Hz)	f_2 (Hz)	Freq. Ratio
Autoparametric tuned	449.3	224.2	2.0
Autoparametric de-tuned	474.6	224.2	2.1

Figures 8 and 9 illustrate the time domain and FFT of the acceleration input and open circuit output voltage when the excitation frequency is in the vicinity of the resonant frequency of the secondary cantilever. This is the frequency region at which autoparametric resonance of the primary cantilever is theoretically expected to onset under favourable conditions. Both output voltages shown in Figures 8 and 9 are that of the primary cantilever.
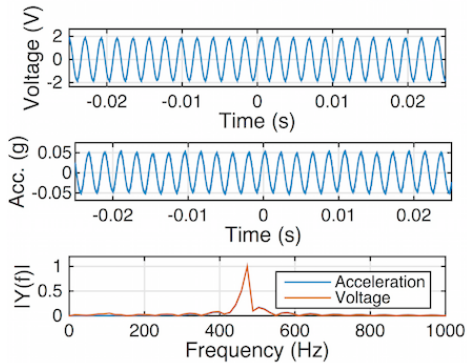

Figure 8: De-tuned device time domain and FFT of the MEMS output (voltage) and vibration input (acceleration), showing just direct resonance.

Figure 8 shows that for the detuned device, the output frequency is the same as the input frequency. This is the response from the direct resonant mode operation coupled from the secondary cantilever. In the FFT domain plot, both the input and output frequency peaks overlap.

On the other hand, figure 9 presents a case where the response frequency of the output voltage is about half the input frequency measured by the accelerometer. This is an evidence of the onset of principal parametric resonance. The FFT plot shows a parametric resonant peak at around 224.2 Hz when the input is at twice the frequency. Furthermore, the primary cantilever also has a small non-resonant response at around 449.3 Hz, coupled in from the clamped resonant oscillation of the secondary cantilever.
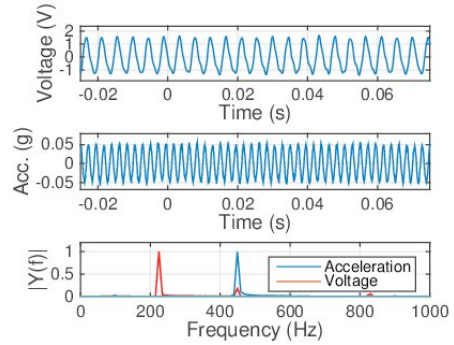

Figure 9: Tuned device time domain and FFT of the MEMS output (voltage) and vibration input (acceleration), showing parametric resonance with a response frequency of 224.2 Hz, which onsets at excitation frequency of 449.3 Hz.

The directly excited resonance in the secondary cantilever is internally coupled to parametrically drive the primary cantilever. In this instance, both the stiffness as well as the effective mass of the primary cantilever is modulated as a function of time when the secondary cantilever oscillates. Figure 10 shows a frequency domain power response of the tuned device across a matched resistive load.
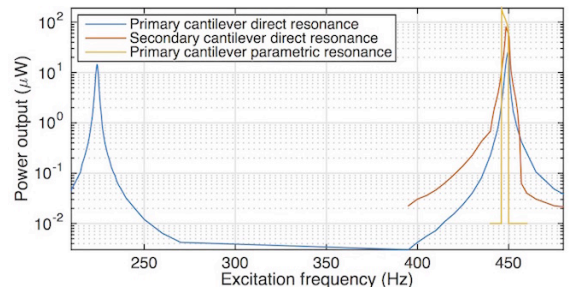

Figure 10: Frequency domain power response at 0.036 g_{rms}. The primary cantilever exhibits 1st mode at 224.2 Hz and coupling from the resonant mode of the secondary cantilever at 449.3 Hz. Furthermore, parametric resonance onsets at around 449.3 Hz.

When excited at 0.036 g_{rms} and measured across a matched resistive load. Parametric resonance for the

primary cantilever attains 180 μW, while direct resonance peaks at 25 μW for the primary cantilever and 80 μW for the secondary cantilever.

The primary cantilever experiences resonant amplifications at: (i) direct resonance, and (ii) parametric resonance. The secondary cantilever on the other hand, only experiences resonant amplification from direct resonance. Under direct resonant excitation, the response from both cantilevers are mutually coupled. However, when the primary cantilever is in parametric resonance, the oscillation of the secondary cantilever is seen to be clamped.

DISCUSSION

As shown in table 2, the autoparametric resonant power density normalised against acceleration squared recorded about an order of magnitude higher than the state-of-the-art [5, 6]. The increase in power density also stems from the piezoelectric MEMS mass optimisation [6] and better matched AlN-to-Si thickness ratio employed here. Further to the transducer and device optimisation, the autoparametric resonant mechanism also offers over two times higher power output than the same device driven into direct resonant response.

Table 2. Comparison of the MEMS device when driven in autoparametric resonance (APR) and direct resonance (DR) with top piezoelectric MEMS devices reported in the literature. P is the average power, Vol. is the effective volume and Acc. is the 0-pk acceleration input. NPD is power density normalised to acceleration squared.

Ref.	Freq. (Hz)	P (μW)	Vol. (cm^3)	Acc. (ms^{-2})	NPD (μW·cm^{-3}·m^{-2}·s^4)
APR	449.3	180	0.112	0.5	6.4×10^3
DR	474.6	80	0.112	0.5	2.9×10^3
[6]	210	1.78	0.005	0.6	9.9×10^2
[7]	167	2.74	0.027	0.98	1.1×10^2
[8]	575	60	0.012	19.6	1.3×10^1
[9]	58	128	0.260	9.8	5.1×10^0

Thus, the realisation of autoparametric resonance in a cantilever-based design enables the possibility of effectively applying this alternative resonant amplification phenomenon for piezoelectric MEMS devices, without compromising piezoelectric strain distribution, in order to enhance the efficiency of harvesting kinetic energy.

CONCLUSION

This paper reports a coupled cantilever topology and the first experimental demonstration of an autoparametric oscillator for piezoelectric MEMS vibration energy harvesting without compromising the transducer strain energy distribution. For a well tuned device with an internal frequency ratio of 2.0:1, autoparametric resonance was observed and exhibited an average power output of 180 μW at 0.036 g$_{rms}$. This translates to a power density normalised against acceleration squared of

6.4×10^3 μW·cm^{-3}·m^{-2}·s^4, which is nearly an order of magnitude higher than the state-of-the-art in the literature. Future work will address continued device and transducer optimisation, as well as development of suitable stopper mechanisms [10] within a wafer-level package to improve reliability under large amplitude vibration representative of practical applications.

ACKNOWLEDGEMENTS

REFERENCES

[1] Y. Jia, J. Yan, K. Soga and A.A. Seshia, "Parametrically excited MEMS vibration energy harvesters with design approaches to overcome initiation threshold amplitude", *J. Micromech. Microeng.*, vol. 23, no. 11, 10pp, 2013.

[2] Y. Jia, J. Yan, K. Soga and A.A. Seshia, "Multi-frequency operation of a MEMS vibration energy harvester by accessing five orders of parametric resonance", *J. Phys. Cof. Ser.*, vol. 476, no. 1, pp. 607-611, 2013.

[3] Y. Jia, J. Yan, K. Soga and A.A. Seshia, "Parametric resonance for vibration energy harvesting with design techniques to passively reduce the initiation threshold amplitude", *Smart Mater. Struct.*, vol. 23, 13pp, 2014.

[4] Y. Jia and A.A. Seshia, "An auto-parametrically excited vibration energy harvester", *Sens. Actuator A.*, vol. 220, pp. 69-75, 2014.

[5] M.C. Cartmell, *Introduction to linear, parametric and non-linear vibration*, Springer Netherlands, 1990.

[6] Y. Jia, A.A. Seshia, "Power Optimisation by Mass Tuning for MEMS Piezoelectric Cantilever Vibration Energy Harvesting", *J. Microelectromech. Syst.*, vol. 25, no. 1, pp. 108-117, 2015

[7] E. Aktakka, R. Peterson and K. Najafi, "Thinned-PZT on SOI process and design optimization for piezoelectric inertial energy harvesting", in *Digest Tech. Papers Transducers'11 Conference*, Beijing, June 5-9, pp. 1649-1652, 2011.

[8] R. Elfrink, V. Pop, D. Hohlfeld, T. M. Kamel, S. Matova, C. de Nooijer, M. Jambunathan, M. Goedbloed, L. Caballero, M. Renaud, J. Penders and R. van Schaijk, "First autonomous wireless sensor node powered by a vacuum-packaged piezoelectric MEMS energy harvester", in *Digest Tech. Papers IEDM'09 Conference*, Baltimore, December 7-9, pp. 543-546, 2009.

[9] R. Andosca, T.G. McDonald, V. Genova, S. Rosenberg, J. Keating, C. Benedixen and J. Wu, "Experimental and theoretical studies on MEMS piezoelectric vibrational energy harvesters with mass loading", *Sens. Actuators A*, vol. 178, pp. 76-87, 2012.

[10] S.T. Chen, S. Du, E. Arroyo, Y. Jia and A.A. Seshia, "Shock reliability enhancement for MEMS vibration energy harvesters with nonlinear air damping as a soft stopper", *J. Micromech. Microeng.*, vol. 27, no. 10, 13pp, 2017.

CONTACT

Y. Jia, tel: +44-7748-839904; yu.jia.gb@ieee.org